J. Phys. Chem. A **2004,** *108,* 4163−4173

Direct Observation of the Forbidden Hydrogen Atom Adduct to Acetonitrile: A Neutralization−Reionization Mass Spectrometric and CCSD(T) ab Initio/RRKM Study

Xiaohong Chen, Erik A. Syrstad, and František Tureček*

Department of Chemistry, Bagley Hall, Box 351700, University of Washington,
Seattle, Washington 98195-1700

Received: January 27, 2004; In Final Form: February 27, 2004

Collisional neutralization of protonated acetonitrile ($\mathbf{6}^+$) generates (*E*)- and (*Z*)-1-azapropen-2-yl radicals, $CH_3-C^{\bullet}=N-H$, (**3** and **4**, respectively) that represent the kinetically and thermodynamically forbidden adducts of hydrogen atoms to acetonitrile. Radicals **3** and **4** are formed with an excess of internal energy due to Franck−Condon effects and rapidly dissociate by loss of the imine hydrogen atom, a methyl hydrogen, and by $CH_3\cdots C=N-H$ bond cleavage. The branching ratios for the loss of the imine hydrogen (H or D) and methyl group (CH_3 or CD_3) were determined for $CH_3-C^{\bullet}=N-H$, $CD_3-C^{\bullet}=N-H$, $CH_3-C^{\bullet}=N-D$, and $CD_3-C^{\bullet}=N-D$ as 70/30, 66/34, 43/57, and 61/39, respectively. Ab initio calculations with coupled clusters with single, double, and perturbative triple excitations/aug-cc-pVTZ predict the loss of the imine hydrogen from **4** to have the lowest transition-state energy. The calculated branching ratios that were based on Rice−Ramsperger−Kassel−Marcus (RRKM) unimolecular rate constants agreed with the mass spectrometric data within experimental accuracy. However, the loss of the methyl hydrogen is predicted by RRKM to be incompetitive (<0.1%) on the ground doublet electronic states of **3** and **4**. The observed fraction (∼10%) is presumed to occur from an excited electronic state.

Introduction

Additions of small atomic and molecular radicals to unsaturated and aromatic compounds are important in several natural and industrial processes where they can result in hydrogenation, halogenation, oxidation, or alkyl group addition. In particular, radical intermediates of acetonitrile (**1**) have been implicated in connection with its thermolysis,[1] radiolysis,[2,3] catalytic hydrogenation,[4] and amine dehydrogentation,[5] as well as terrestrial[6,7] and planetary atmospheric chemistry.[8] Recently, Wang and co-workers[9] have studied by Gaussian 3 ab initio calculations the potential-energy surface for the addition of hydrogen atom to **1** and identified the 1-azapropen-1-yl radical (**2**) as the kinetically favored product (Scheme 1). These calculations agreed with the results of an earlier experimental study[3] that used electron paramagnetic resonance (EPR) spectroscopy to identify **2** as a transient intermediate of radiolysis of **1**. The computed relative energies were also used by Bondybey and co-workers to assign structure to an H atom adduct produced by the reaction of **1** with hydrated electrons in nanodroplets.[10] Interestingly however, the isomeric (*E*)- and (*Z*)-1-azapropen-2-yl radicals (**3** and **4**, respectively) were found to be both thermodynamically and kinetically disfavored compared to **2**. Radicals **3** and **4** are relevant as potential intermediates of another important reaction, i.e., the addition of methyl and higher alkyl radicals to isocyanic acid (**5**, Scheme 1). This reaction has been suspected to be responsible for the depletion of **5** in the interplanetary space and in the atmosphere of the Saturnian moon Titan.[8] However, Petrie has recently reported complete basis set (CBS)-RAD calculations that showed that the methyl addition proceeds with an activation barrier that would render the reaction extremely slow at low temperatures.[11]

SCHEME 1

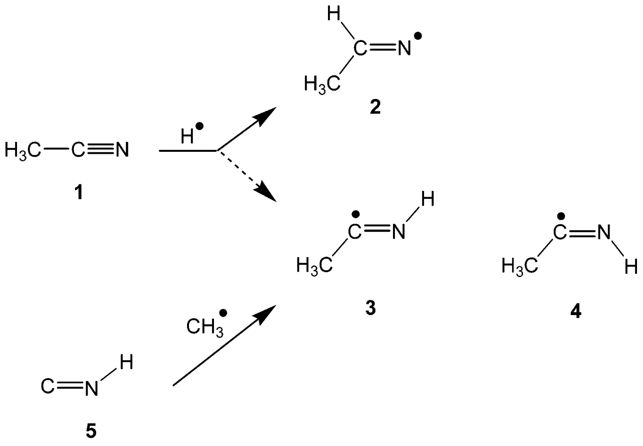

The previous studies have indicated that radical intermediates **3** and **4** are disfavored both kinetically and thermodynamically, and thus represent a challenging goal for an experimental study aimed at their generation and characterization. We now report a direct preparation and characterization of transient 1-azapropen-2-yl radicals in the gas phase. The synthetic route to **3** and **4** is guided by the idea that the inherent reactivity of these radicals is caused by an unfavorable electron distribution due to the presence of an unpaired electron at the imine carbon atom. Therefore, it can be expected that removing the electron would result in an inherently stable cation $\mathbf{6}^+$. Previous calculations and gas-phase ion studies confirm that ion $\mathbf{6}^+$ is a stable species that is readily formed by gas-phase protonation of **1**.[12,13] Cation $\mathbf{6}^+$ can be converted to radicals **3** or **4** by collisional electron transfer from a suitable atomic or molecular donor. This is accomplished by accelerating mass-selected $\mathbf{6}^+$ to a high velocity (182 000 ms^{-1}) and discharging the ion by a glancing collision

---

* To whom correspondence may be addressed. Tel.: (206) 685-2041. Fax: (206) 685-3478. E-mail: turecek@chem.washington.edu.

10.1021/jp040075f CCC: $27.50

SCHEME 2

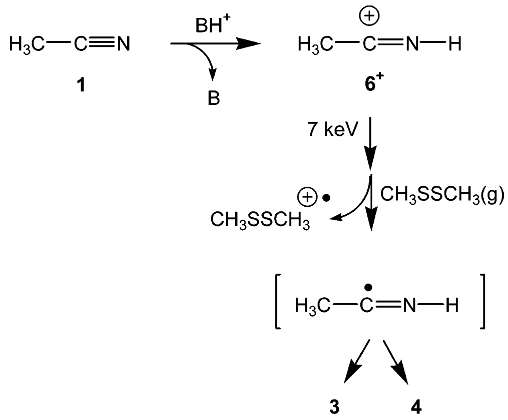

with dimethyl disulfide (DMDS, Scheme 2). The collision kinematics mandates that the electron transfer between DMDS and **6**$^+$ occur within 3×10^{-15} s, which is less than the period of any of the molecular vibrations in **6**$^+$, so that the resulting radical is formed with the geometry of the precursor ion. The radicals are probably formed in a mixture of geometrical isomers (**3**/**4**) that are observed on a microsecond time scale when dissociations occur. Surviving radicals and dissociation products are identified following nonspecific collisional reionization and mass analysis. This neutralization−reionization (NR) mass spectrometric method[14] has been used extensively for the generation of a number of elusive neutral species, molecules, radicals, carbenes, biradicals, etc., as reviewed.[15] Isotope labeling in **6a**$^+$−**6d**$^+$ is used to determine the dissociation mechanisms in the radicals formed therefrom.

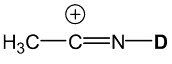
$H_3C-\overset{\oplus}{C}=N-D$

6a$^+$

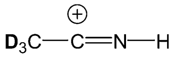
$D_3C-\overset{\oplus}{C}=N-H$

6b$^+$

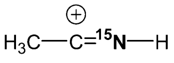
$H_3C-\overset{\oplus}{C}={}^{15}N-H$

6c$^+$

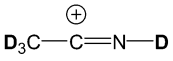
$D_3C-\overset{\oplus}{C}=N-D$

6d$^+$

The experimental results are complemented by ab initio calculations at high levels of theory that provide reaction and transition-state energies for **3** and **4** that are further used for Rice−Ramsperger−Kassel−Marcus (RRKM)[16] calculations of rate constants to obtain branching ratios.

Experimental Section

Materials. Acetonitrile and DMDS (both reagent grade) were purchased from Sigma-Aldrich and used as received. CD_3CN, CD_3OD (99% D), and $CH_3C^{15}N$ (99% ^{15}N) were all purchased from Cambridge Isotope Laboratories. CH_4 (99.99% pure) and CD_4 (99% D) were purchased from Matheson.

Methods. NR mass spectra were measured on a tandem quadrupole acceleration−deceleration mass spectrometer described previously.[17] Ions were prepared in an electron impact or a chemical ionization ion source.[18] The source conditions were as follows: emission current, 500 μA for EI and 1 mA for the chemical ionization (CI); the electron energy was tuned for the best signal but typically was 70 eV for the EI source and 100 eV for the CI source; the source temperature was 200−220 °C. Acetonitrile was degassed by several freeze−pump−thaw cycles and introduced into the ion source from a glass liquid probe at room temperature. However, due to the high volatility, acetonitrile was immersed in an ice−water bath throughout each experimental period in order to keep the partial pressure stable. CH_4, CD_4, CH_3OH, and CD_3OD were used as CI reagent gases at pressures $1.0-2.0 \times 10^{-4}$ Torr as read on an ionization gauge located at the diffusion pump intake. The ions were extracted from the source, transmitted through a radiofrequency-only quadrupole filter, accelerated to 7250 eV by a special lens, and focused on a collision cell floated at −7170 V, where DMDS vapor was admitted at pressures such as to achieve 70% transmission of the ion beam. Residual ions and neutrals were allowed to drift to a four-segment conduit maintained at +250 V that reflected the ions while allowing the neutrals to pass through. Neutrals were reionized by collisions with oxygen at pressures allowing 70% beam transmittance. The ions formed were decelerated to 75−80 eV, energy filtered, and analyzed by a quadrupole mass filter that was operated at unit mass resolution. The instrument was tuned daily to match the reference NR mass spectrum of CS_2. Typically, 100 repetitive scans were accumulated per spectrum at a 1 mass unit/s scan rate, corresponding to 200 data points per peak. Variable-time NR mass spectra were measured as described previously,[19] only −7 kV was used instead of −8 kV to match up the acceleration voltage supplied. Repetitive scans (300) were accumulated per a variable-time NR mass spectrum.

Calculations. Standard ab initio and density functional theory calculations were performed using the Gaussian 98 suite of programs.[20] Geometries were optimized with Becke's hybrid functional (B3LYP)[21] and the 6-311++G(2d,p) basis set. Spin-unrestricted calculations (UB3LYP, UMP2, UQCISD(T), and UCCSD(T)) were used for open-shell systems. In the UB3LYP calculations, $\langle S^2 \rangle$ operator expectation values ranged from 0.751 to 0.767 and 0.764 to 0.766 for local minima and transition states, respectively. Contamination by higher spin states in UMP2 calculations was treated by a standard annihilation procedure.[22] The energy corrections upon spin annihilation in the effective QCISD(T)/6-311++G(3df,2p) energies were ≤ 0.5 millihartree (1.3 kJ mol^{-1}) and 0.24 millihartree root-mean-square deviation for the entire set, with the exception of $CH_3CN^{\bullet+}$, where the correction was 22 millihartree. Optimized structures were characterized by harmonic frequencies as local minima (all real frequencies) and saddle points (one imaginary frequency). The optimized geometries are available as Supporting Information. Improved energies were obtained by single-point calculations using the Gaussian 2 (MP2)[23] and Gaussian 2[24] schemes. Another set of QCISD(T) energies were obtained in a fashion that is analogous to G2 (MP2) by expanding the basis set from 6-311G(d,p) to 6-311++G(3df,2p) through spin-projected PMP2/6-311++G(3df,2p) single-point calculations. This expansion corresponds to effective QCISD(T)/6-311++G-(3df,2p) calculations. On our highest level of theory, single-point coupled-cluster calculations[25] with single, double, and perturbational triple excitations of valence electrons (CCSD-(T)[26] were carried out with Dunning's correlation-consistent basis set of a triple-ζ quality equipped with polarization and diffuse functions on all atoms, CCSD(T)/aug-cc-pVTZ.[27] Transition-state geometries were obtained by mapping the relevant parts of the potential-energy surface with B3LYP/6-311++G-(2d,p) calculations in which one internal coordinate was chosen as a reaction coordinate and was varied stepwise, while the other internal coordinates were fully optimized. Single-point energies were calculated by effective QCISD(T)/6-311++G(3df,2p) at all points along the reaction path, and the refined potential-energy surface was fitted with a 4th-order polynomial to locate

TABLE 1: Ion Relative Energies

Reaction	relative energy[a,b] B3LYP	G2(MP2)	CCSD(T)[c]
$CH_3C{=}N{-}H$ (**6**$^+$) → CH_3CN (**1**) + H^+	782 (787)[d]	777 (782)[d]	777 (782)[d]
$CH_2{=}C{=}NH_2^+$ (**7**$^+$) → $CH_2{=}C{=}NH$ (**8**) + H^+	825	823	824
$CH_3N{=}C{-}H^+$ (**9**$^+$) → CH_3NC + H^+	830 (836)[d]	830 (836)[d]	
6$^+$ → **7**$^+$	52 (51)[d]	69 (69)[d]	67 (67)[d]
6$^+$ → **9**$^+$	51 (51)[d]	44 (44)[d]	
6$^+$ → **TS** → **7**$^+$	525	521	
1 + **1**$^{\bullet+}$ → **6**$^+$ + $CH_2CN^\bullet$	−226	−254	−235
6$^+$ + CH_3CN → $CH_3C{=}NCH_3$ (**10**$^+$) + $C{=}N{-}H$	49 (42)[d]	46 (38)[d]	
9$^+$ + CH_3CN → $CH_3C{=}NCH_3$ (**10**$^+$) + $H{-}CN$	−58 (−56)[d]	−54 (−52)[d]	
6$^+$ → **1**$^{\bullet+}$ + $H^\bullet$	608	645	631
6$^+$ → **8**$^{\bullet+}$ + $H^\bullet$	404	413	
$CH_3CN\cdots H^+...NCCH_3$ → $CH_2{=}C{=}NH_2...H^+...NCCH_3$	87	101	

[a] In units of kJ mol^{-1}. [b] At 0 K, including B3LYP/6-311++G(2d,p) zero-point corrections. [c] From single-point calculations with the aug-cc-pVTZ basis set. [d] Proton affinities and relative enthalpies at 298 K.

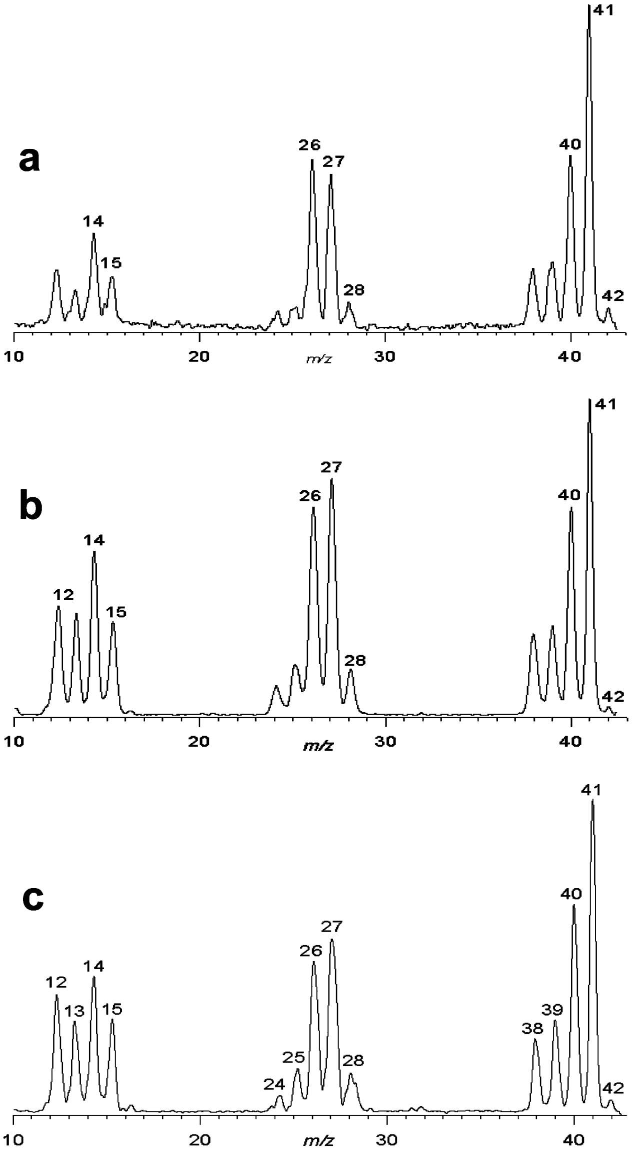

Figure 1. Neutralization (CH_3SSCH_3, 70% transmittance)/reionization (O_2, 70% transmittance) mass spectra of **6**$^+$ from (a) CH_3OH CI, (b) CH_4 CI, and (c) self-CI.

the saddle-point geometry. Single-point CCSD(T)/aug-cc-pVTZ calculations were then used to obtain potential energies in transition states that were corrected for zero-point vibrational contributions.

Excited-state energies were calculated using time-dependent density functional theory[28] with B3LYP/6-311++G(2d,p). The ($^2A''$) ***A*** state in **3** was optimized by MP2/6-311++G(2d,p). The initial guess for the wave function in the $^2A''$ state was obtained by promoting an electron from the 12α singly occupied orbital (10a′) to a virtual orbital of A″ symmetry (6a″) that was found by configuration interaction singles (CIS)[29] calculations to have the largest element in the CI matrix. Attempts at CIS/6-311++G(2d,p) geometry optimizations of excited states in **3** were unsuccessful as the calculations oscillated between different roots of the CIS matrix and did not achieve convergence.

RRKM calculations were performed using Hase's program[30] that was recompiled for Windows NT.[31] Unimolecular rate constants were obtained by a direct count of quantum states at internal energies that were increased in 2-kJ mol^{-1} steps from the transition state up to 350 kJ mol^{-1} above the reactant. Rotations were treated adiabatically, and the calculated $k(E,J,K)$ rate constants were Boltzmann averaged over the thermal distribution of rotational states at 473 K, corresponding to the ion-source temperature.

Results and Discussion

Ion Preparation and Dissociations. NR mass spectrometric studies of transient neutral intermediates rely on an unambiguous preparation of gas-phase ion precursors of well-defined structures.[15] A straightforward route to ion **6**$^+$ is by protonation of acetonitrile (**1**) using a gas-phase acid (BH^+) such that the proton affinity of its conjugate base (B) is lower than the proton affinity of **1** (779 kJ mol^{-1})[32−34] to make the proton transfer exothermic. In this study, we used $CH_3OH_2^+$, CH_5^+, and $CH_3CN^{\bullet+}$ as gas-phase acids in chemical ionization (CI),[35] denoted as CH_3OH-CI, CH_4-CI, and self-CI, according to eqs 1−3[33,34]

$$CH_3CN + CH_3OH_2^+ \rightarrow CH_3C{=}N{-}H^+ + CH_3OH \; \Delta H_{rxn,298} = -25 \text{ kJ mol}^{-1} \quad (1)$$

$$CH_3CN + CH_5^+ \rightarrow CH_3C{=}N{-}H^+ + CH_4 \Delta H_{rxn,298} = -236 \text{ kJ mol}^{-1} \quad (2)$$

$$CH_3CN + CH_3CN^{\bullet+} \rightarrow CH_3C{=}N{-}H^+ + {}^\bullet CH_2CN \Delta H_{rxn,298} = -247 \text{ kJ mol}^{-1} \quad (3)$$

Protonation with $CH_3OH_2^+$ is only mildly exothermic. If we assume that the reaction enthalpy in eq 1 is partitioned between CH_3OH ($C_{v,473}$ = 41 J mol^{-1} K^{-1}) and **6**$^+$ ($C_{v,473}$ = 61 J mol^{-1} K^{-1}) according to their rovibrational heat capacities ($C_{v,473}$),

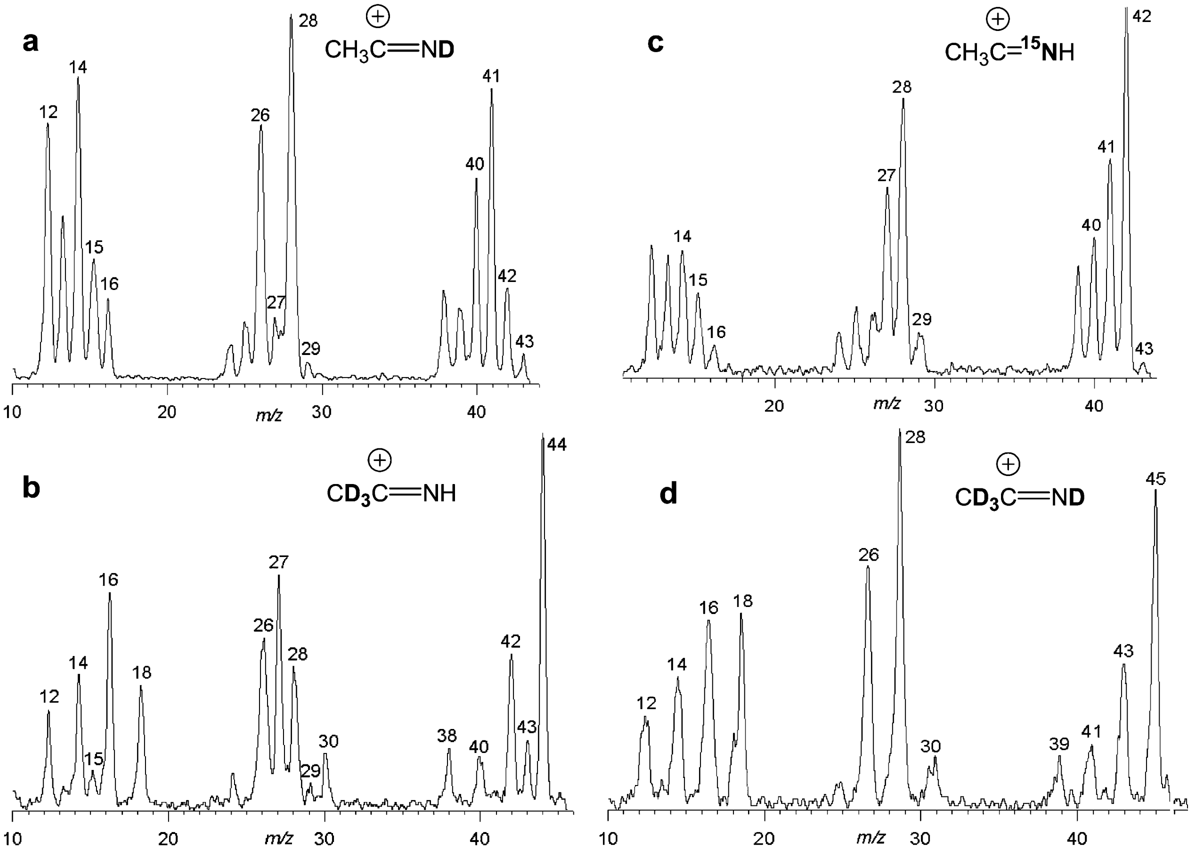

Figure 2. Neutralization (CH_3SSCH_3, 70% transmittance)/reionization (O_2, 70% transmittance) mass spectra of (a) **6a**$^+$, (b) **6b**$^+$, (c) **6c**$^+$, and (d) **6d**$^+$. The precursor ions were prepared by CD_3OD CI (a and d) and CH_3OH CI (b and c).

ion **6**$^+$ receives 15 kJ mol^{-1}, so that its mean internal energy can be estimated at $E = H_{473}(\mathbf{1}) + 15 = 27$ kJ mol^{-1}, which only slightly exceeds the thermal value, H_{473} (**6**$^+$) = 16 kJ mol^{-1}, at the same ion-source temperature (473 K). Energy equilibration can be aided by the formation of a stable proton-bound complex of **1** and methanol.[36] In contrast, protonations with CH_5^+ and $CH_3CN^{\bullet+}$ are substantially exothermic and can be expected to produce hyperthermal **6**$^+$, despite partial energy dissipation by several tens of collisions with neutral molecules that the ion undergoes during its residence time in the ion source.[15] Importantly however, **6**$^+$ is the lowest-energy structure among the $C_2H_4N^+$ isomers[37] and the only one accessible directly by protonation of **1**. Table 1 energies show that the second most stable $C_2H_4N^+$ isomer with the C−C−N frame (**7**$^+$) is 67 kJ mol^{-1} less stable than **6**$^+$ and would be negligibly populated in the gas-phase equilibrium at 473 K. Unimolecular isomerization $\mathbf{6}^+ \rightarrow \mathbf{7}^+$ requires a prohibitively high transition-state energy (521 kJ mol^{-1}). Furthermore, a proton-bound complex of **7**$^+$ with **1** is 101 kJ mol^{-1} less stable than a complex of **6**$^+$, indicating that formation **7**$^+$ is not facilitated in ion−molecule complexes. Note also that protonation at the middle carbon atom in **1**, which would correspond to an ionized form of **2**, does not form a stable structure. Hence, the energy data suggest that the desired isomer **6**$^+$ is the only $C_2H_4N^+$ species produced by protonation of **1**.[38]

Formation and Dissociations of Radicals 3 and 4. Collisional neutralization of **6**$^+$ followed by reionization of neutral intermediates produced the mass spectra shown in Figure 1. Since we cannot distinguish experimentally the geometrical isomers **3** and **4**, these are referred to as **3/4** throughout this section. The spectra show a minor peak of a survivor ion at *m*/*z* 42 that corresponds to reionization of C_2H_4N radicals, presumably **3/4**. That a fraction of **3/4** is indeed observed and not due to contamination by isotopes from residual $\mathbf{1}^{\bullet+}$ is confirmed by the NR mass spectrum of $CH_3C{=}ND$ (**6a**$^+$) that shows a peak at *m*/*z* 43. To minimize isotope contamination, we carried out gas-phase protonations under conditions that secured high (>95%) conversions to achieve $[C_2H_4N^+]/[C_2H_3N^+]$ ratios greater than 20. Because of the presence of stable ^{13}C and ^{15}N isotopes in $\mathbf{1}^{\bullet+}$ at their natural abundance, the contribution of combined ($^{13}C + {}^{15}N$) satellites of $C_2H_3N^{\bullet+}$ was $(1/20) \times (2.2 + 0.37) = 0.13\%$ at *m*/*z* 42 in **6**$^+$, but only $(1/20) \times (0.0121 + 0.020) = 0.0016\%$ at *m*/*z* 43 in **6a**$^+$. Thus, if most of the survivor ion at *m*/*z* 42 from **6**$^+$ were due to isotopic contamination, no survivor ion would have been detected at *m*/*z* 43 from **6a**$^+$, contrary to observations. The relative abundance of survivor ions was found to depend on the precursor-ion internal energy, dissociation time, and isotope content. For example, whereas the NR mass spectra of **6**$^+$, **6a**$^+$, **6b**$^+$, and **6c**$^+$ showed survivor ions of comparable relative intensities, the spectrum of $CD_3C{=}ND^+$ (**6d**$^+$) showed a negligibly small peak at *m*/*z* 46 due to a survivor ion. The other effects are discussed later in the paper.

The NR mass spectra are dominated by dissociation products belonging to three groups. The *m*/*z* 38−41 group arises from reionization of **1** and its $CH_2{=}C{=}NH$ isomer (**8**) followed by their ion dissociations. This assignment is supported by deuterium labeling that shows loss of D (major) and H (minor) from $CH_3C{=}ND$ (**3a/4a**), produced by neutralization of labeled ion **6a**$^+$ (Figure 2a), and also by complementary losses of H (major) and D (minor) from $CD_3C{=}NH$ (**3b/4b**), produced by neutralization of ion **6b**$^+$ (Figure 2b). The second group at *m*/*z* 24−28 consists of C_2, C_2H, and partially overlapping C_2H_x ($x = 2-4$) and CNH_x ($x = 0-2$) fragments. The overlaps at *m*/*z* 26−28 were deconvoluted by deuterium and ^{15}N labeling. In particular, the NR mass spectrum of $CH_3C{=}^{15}NH^+$ (**6c**$^+$, Figure 2c) shows shifts of *m*/*z* 26 → *m*/*z* 27, *m*/*z* 27 → *m*/*z* 28, and *m*/*z* 28 → *m*/*z* 29, indicating that the majority of these fragments contain nitrogen and correspond to CNH_x. Likewise, the NR mass spectrum of $CD_3C{=}NH^+$ (**6b**$^+$, Figure 2b) shows CN and CNH at *m*/*z* 26 and 27, whereas the hydrocarbon fragments are shifted to *m*/*z* 28 and 30 for C_2D_2 and C_2D_3, respectively. Finally, the group at *m*/*z* 12−15 corresponds to C, CH, and partially overlapping peaks of CH_x ($x = 2,3$) and NH_x ($x = 0,1$). The presence of NH is confirmed by the peaks at *m*/*z* 16 in the NR mass spectra of **6a**$^+$ (ND) and **6c**$^+$ (^{15}NH), and by the peak at *m*/*z* 15 (NH) from **6b**$^+$. The product analysis indicates that loss of H and CH_3 are the main dissociations of radicals **3**/**4**, as summarized in Scheme 3.

SCHEME 3

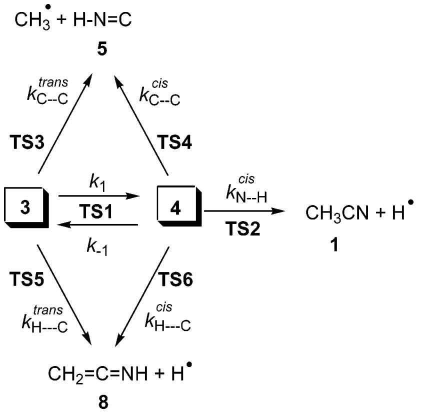

Effects of Precursor Ion Energy and Neutral Dissociation Time. We further investigated the effects on the NR mass spectra of the internal energy in **6**$^+$ and its isotopomers. Ions **6**$^+$ prepared by exothermic protonations in CH_4 CI (Figure 1b) and self-CI (Figure 1c) (eqs 2 and 3) showed more extensive dissociations in the corresponding NR mass spectra compared to those formed by CH_3OH CI (Figure 1a). In particular, the relative abundance of the **3**/**4** survivor peak was highest in the NR mass spectrum of **6**$^+$ from CH_3OH CI. Similar effects were observed for **6a**$^+$, where the NR mass spectrum of **6a**$^+$ from CD_3OD CI shows a more abundant survivor peak at *m*/*z* 43 than does the spectrum of the ion from CD_4 CI (Figure 3a). However, an increase in the survivor ion relative intensity was also observed when ion **6a**$^+$ was generated by CD_4 CI at a lower ion-source pressure (Figure 3b). Under “low pressure” CI, ion **6a**$^+$ undergoes fewer collisions and is expected to retain a larger portion of the internal energy acquired by exothermic proton transfer (eq 2).

We have also studied the temporal dependence of the product ion relative intensities in the NR mass spectra of **6a**$^+$ produced by CD_3OD CI (Figure 4). The variable-time NR mass spectra show changes mainly in the [*m*/*z* 40]/[*m*/*z* 41] abundance ratios that decrease as the neutral dissociation times are increased from 0.3 to 3.3 μs. Since in these measurements the ion dissociation times are shortened by the same amount (3 μs), more dissociation at longer ion drift times indicates that the consecutive losses of H atoms are due to ion dissociations occurring after reionization. It is also noteworthy that the relative intensity of the survivor ion did not increase at short neutral dissociation times.

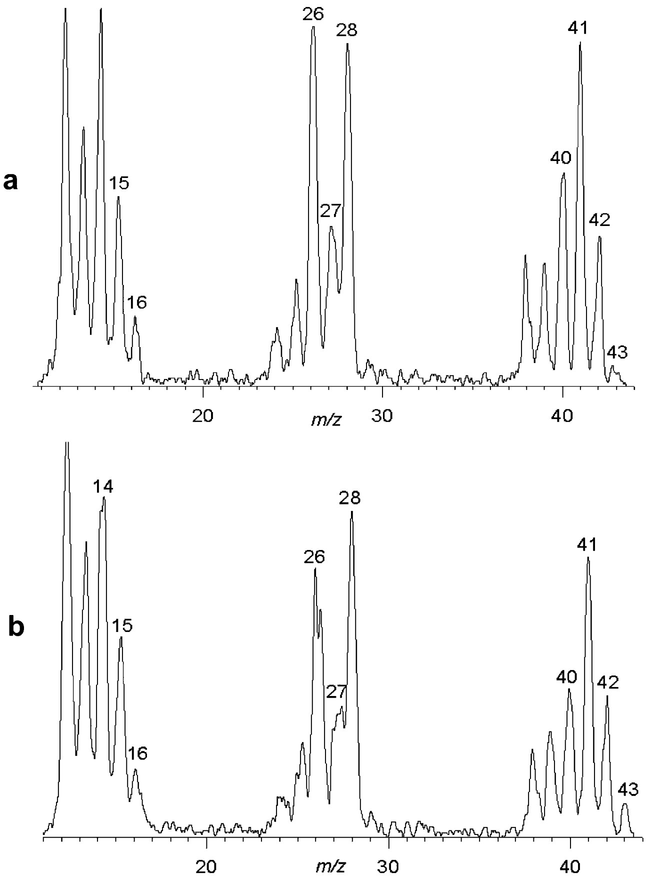

Figure 3. Neutralization (CH_3SSCH_3, 70% transmittance)/reionization (O_2, 70% transmittance) mass spectra of **6a**$^+$ prepared at high (a, 1.2×10^{-4} Torr) and low (b, 8.5×10^{-5} Torr) CD_4 pressure in the ion source.

Characterization of Dissociation Products. To quantify the dissociations of **3**/**4** and obtain experimental branching ratios, we measured reference NR mass spectra of some of the products. Acetonitrile (**1**) is a stable molecule whose NR mass spectra were measured under two different conditions. First, ion **1**$^{\bullet+}$ was neutralized by collisions with DMDS to give the spectrum shown in Figure 5a. The electron transfer between **1**$^{\bullet+}$ and DMDS is highly exothermic, judged from the difference in the ionization energies, $\Delta IE = 12.2-8.1 = 4.1$ eV,[33,39] and can be expected to form a fraction of **1** in excited electronic and vibrational states. In contrast, neutralization with Xe is nearly thermoneutral, $\Delta IE = 12.20-12.13 = 0.07$ eV,[32] and is expected to form less energetic **1** in which some vibrational excitation can be due to Franck−Condon effects.[40] The NR mass spectrum of thus prepared **1**$^{\bullet+}$ (Figure 5b) shows substantially less fragmentation than does the spectrum in Figure 5a. We consider neutral molecules of **1** that were generated under parts a and b of Figure 5 conditions to represent two extreme cases of hot and cold acetonitrile. Thus, the NR fragmentations of **1** of unknown internal energy, as produced by H loss from **3**/**4**, can be represented as a linear combination of the spectra in parts a and b of Figure 5. The normalized NR ion intensities from the spectra in parts a and b of Figure 5 were mixed and subtracted from the normalized ion intensities in the NR mass spectra of **6**$^+$, so as to annihilate within ±0.6% the peaks at *m*/*z* 38−41, which mainly correspond to reionized **1**. A similar procedure was used for assessing the contribution of deuterium-labeled acetonitrile formations from **6a**$^+$, **6b**$^+$, and **6d**$^+$. The ion intensities in the difference spectra, NR(**6**$^+$) − NR(**1**$^{\bullet+}$), were assigned to being due to CH_3 and $H{-}N{=}C$ and likewise for the corresponding labeled isotopomers. Because $H{-}N{=}C$ (**5**) and $D{-}N{=}C$ are unstable molecules, we were unable to obtain their reference NR mass spectra. An NR mass spectrum of DCN was obtained and showed mainly the survivor ion at *m*/*z* 28 and minor fragments at *m*/*z* 26 (CN) and 14 (N + DC). A C_2H_3N isomer, presumably $CH_2{=}C{=}NH$ (**8**), which is formed by loss

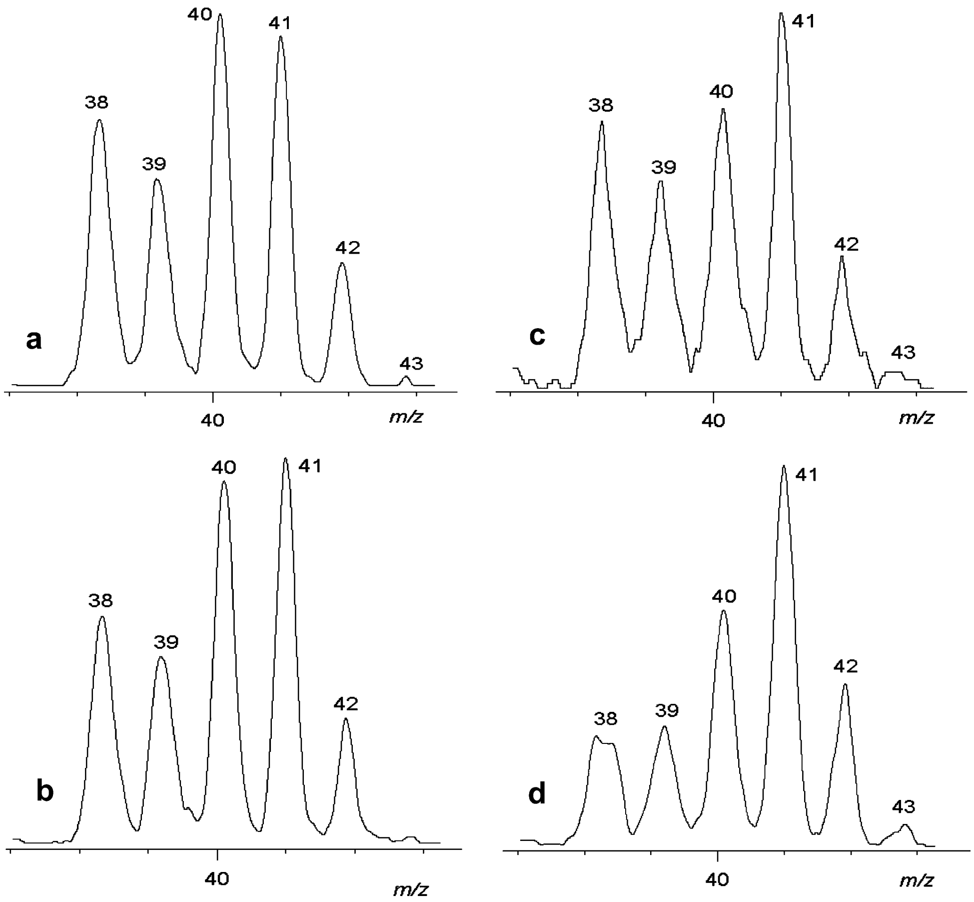

Figure 4. Variable-time NR mass spectra (*m/z* 36−44 region) of **6a**$^+$. The neutral dissociation times were (a) 0.3 μs, (b) 0.9 μs, (c) 1.6 μs, and (d) 3.3 μs.

TABLE 2: Experimental Branching Ratios for Losses of (H,D) and (CH_3,CD_3) from 3/4−3d/4d

reactant[a]	loss of (H,D) from N−(H,D)	loss of (CH_3,CD_3)
$CH_3C{=}N{-}H$ (**3/4**)	70	30
$CH_3C{=}N{-}D$ (**3a/4a**)	43	57
$CD_3C{=}N{-}H$ (**3b/4b**)	66	34
$CD_3C{=}N{-}D$ (**3d/4d**)	61	39

[a] For precursor ions by methanol CI.

of a methyl H from **3/4**, is another unstable molecule for which we did not have a reference NR mass spectrum. From the difference NR mass spectra of **6a** and **6b**, we estimate the formation of **8** at ≤10% of **1**.

The integrated NR ion intensities corresponding to **1** and (CH_3 + H−N═C) were further scaled by their ionization cross sections which were estimated from the Fitch−Sauter scheme for electron ionization.[41] The scaled total ion intensities were used to estimate the branching ratios for the loss of H and CH_3 from **3/4** (Table 2). The experimental data show a 70/30 branching ratio for the loss of H and CH_3 from **3/4**. Primary isotope effects lower the branching ratio to 43/57 for the loss of D and CH_3 from **3a**/**4a**, while secondary isotope effects are small and result in branching ratios equal to 66/34 for the loss of H and CD_3 from **3b**/**4b**, and 61/39 for the loss of D and CD_3 from **3d**/**4d**. The data indicate that loss of H is slightly favored from **3/4**, but loss of CH_3 is competitive under NR experimental conditions.

Radical Dissociation and Transition State Energies. To interpret the experimental data, we carried out ab initio calculations of radicals **3**, **4**, and transition states for their dissociations and isomerizations. These calculations were in part guided by the previous work of Wang et al.[9] and Petrie[11] that included several relevant geometries that were optimized at comparable levels of theory. The computational results are therefore discussed only briefly here. The energies calculated at the CCSD(T)/aug-cc-pVTZ level of theory are discussed in the text; those from the other levels of theory are summarized in Table 3.

The dissociation of the N−H bond reaches a transition state (**TS2**, E_{TS2} = 83 kJ mol^{-1}) that has a cis arrangement of the departing H atom and the methyl group. In contrast, a transoid geometry is not a true transition state[9] so that the loss of the imine hydrogen in **3** must proceed through isomerization to **4** through **TS1** at 68 kJ mol^{-1} above **3**. Figure 6 shows that **TS2** is reasonably well represented on the B3LYP potential-energy surface at d(N−H) = 1.621 Å. The effective QCISD(T)/6-311++G(3df,2p) and CCSD(T) potential-energy surfaces along the reaction path are very similar to each other, with **TS2** occurring at a somewhat shorter separation, d(N−H) = 1.533 Å. It may be noted that the B3LYP potential-energy surface rather severely underestimates the activation energy for the addition of H to **1** by overestimating the energy for CH_3CN + H.

More significant differences were obtained for potential-energy surfaces for the C−C bond cleavages in **3** and **4** (Figure 7). These show distinct transition states for **3** and **4**, **TS3** and **TS4**, respectively. The B3LYP potential-energy surface for the dissociation of **3** has **TS3** at a 2.33 Å C−C separation, as confirmed by frequency analysis. However, at C−C separations past **TS3**, the B3LYP potential-energy surface of **3** develops a discontinuity and collapses to the underlying surface for the

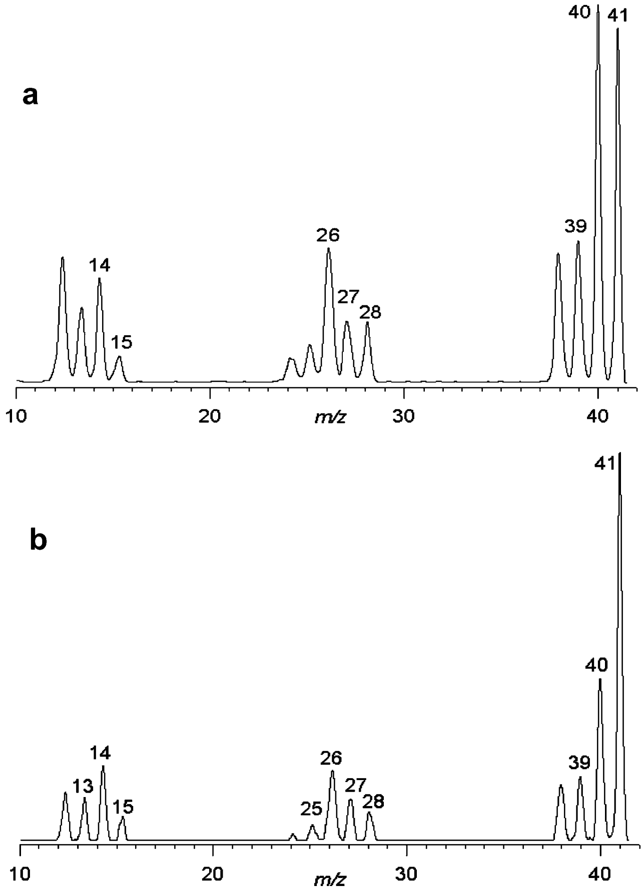

Figure 5. Neutralization (70% transmittance)/reionization (O_2, 70% transmittance) mass spectra of $\mathbf{1}^{\bullet+}$. The neutralization gases were (a) CH_3SSCH_3 and (b) Xe.

C−C bond dissociation in **4** which has a lower transition state at about the same C−C separation (**TS4**, 2.34 Å). These difficulties are absent in potential-energy mapping by effective QCISD(T) or CCSD(T) that both show well-defined transition states at d(C−C) = 2.263 Å (**TS3**, E_{TS3} = 140 kJ mol^{-1}) and 2.245 (**TS4**, E_{TS4} = 117 kJ mol^{-1}). The CCSD(T) activation energy for a CH_3 addition to H−N═C is 35 kJ mol^{-1}.

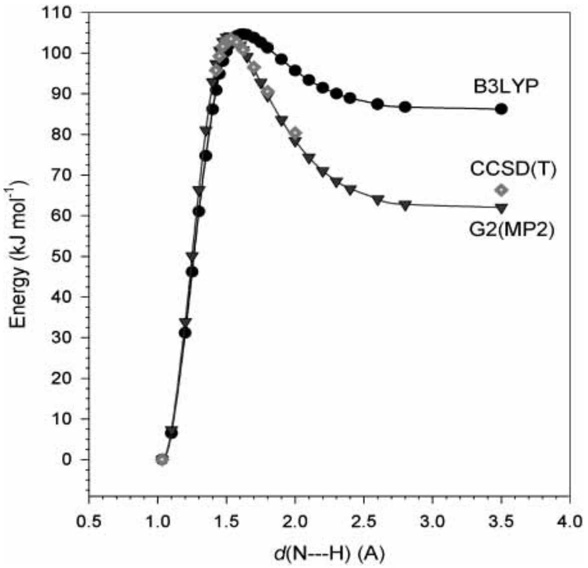

Figure 6. Potential-energy surfaces along the pathway for N−H bond dissociation in **4**. The energies are not corrected for zero-point contributions.

The B3LYP potential-energy surface for the H−C bond dissociation in **3** shows a continuously increasing energy profile to the products, **8** + H (Figure 8). However, this is disproved by the effective QCISD(T)/6-311++G(3df,2p) potential-energy surface which has a well-defined transition state (**TS5**) at d(H−C) = 1.951 Å, in line with single-point CCSD(T) calculations (E_{TS5} = 191 kJ mol^{-1}, Table 3). The high-level calculations thus indicate a 13-kJ mol^{-1} activation energy for the H atom addition to **8**. The H−C bond dissociation in **4** through **TS6** is analogous to the same dissociation of **3** (Figure S2, Supporting Information). The transition state (**TS6**) was found at 1.905 Å on the effective QCISD(T)/6-311++G(3df,2p) potential-energy surface, and its CCSD(T) + ZPVE energy was E_{TS6} = 173 kJ mol^{-1} above **4** (193 kJ mol^{-1} above **3**).

Franck−Condon Effects. Another important feature that is pertinent to NR mass spectra is the internal energy that the radicals receive upon collisional electron transfer. For endothermic collisions at keV kinetic energies, the internal energy of the transient neutral species consists of the precursor ion

TABLE 3: Relative Energies for Neutral Molecules and Radicals

	relative energy[a,b]						
reaction	B3LYP/-6-311++G(2d,p)	QCISD(T)/-6-311++G(3df,2p)[c]	G2(MP2)	G2	CCSD(T)/-aug-cc-pVTZ	ref 11	ref 9
3 → **4**	18	20	20	19	20	19	19
3 → **TS1** (**4**)	65	67			68	67	68
3 → CH_3CN + H$^\bullet$	82	59	59	60	63	61	55
4 → **TS2** (B3LYP)[d]	84	80	81	81	80	78	95
4 → **TS2** (QCISD(T))[e]		84	84	84	83		
3 → $CH_3^\bullet$ + H−N═C	111	99			101	106	102
3 → **TS3** (B3LYP)[d]	140	138			137		
3 → **TS3** (QCISD(T))[e]	138	143	143	145	140		
4 → **TS4** (B3LYP)[d]	120	116			115	117	118
4 → **TS4** (QCISD(T))[e]	119	119	119	121	117		
3 → **8** (CH_2═C═NH) + H$^\bullet$	177	174			178		
3 → **TS5**	177[f]	190			191		
4 → **TS6**	159[f]	173			173		
3 → $CH_3^\bullet$ + HCN	55	44			44		
CH_3CN → $CH_2CN^\bullet$ + H$^\bullet$	382 (388)[g]	393 (399)[g]	393	391	397 (403)[g]		
CH_3CN → CH_2═C═NH	95	115			115		

[a] In units of kJ mol^{-1}. [b] Including B3LYP/6-311++G(2d,p) zero-point corrections and referring to 0 K. [c] Effective single-point energies: E[QCISD(T)/6-311++G(3df,2p)] ≈ E[QCISD(T)/6-311G(d,p)] + E[PMP2/6-311++G(3df,2p)] − E[PMP2/6-311G(d,p)]. [d] Transition states optimized with B3LYP/6-311++G(2d,p). [e] Transition states from fitting the effective QCISD(T)/6-311++G(3df,2p) potential-energy surfaces. [f] Same as the product threshold energy. [g] Dissociation energies at 298 K.

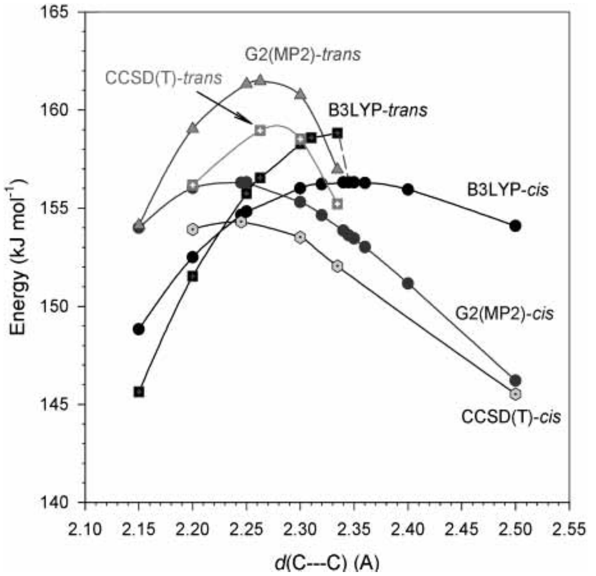

Figure 7. Potential-energy surfaces along the pathway for CH_3-C bond dissociation in **3** and **4**. The energies are not corrected for zero-point contributions.

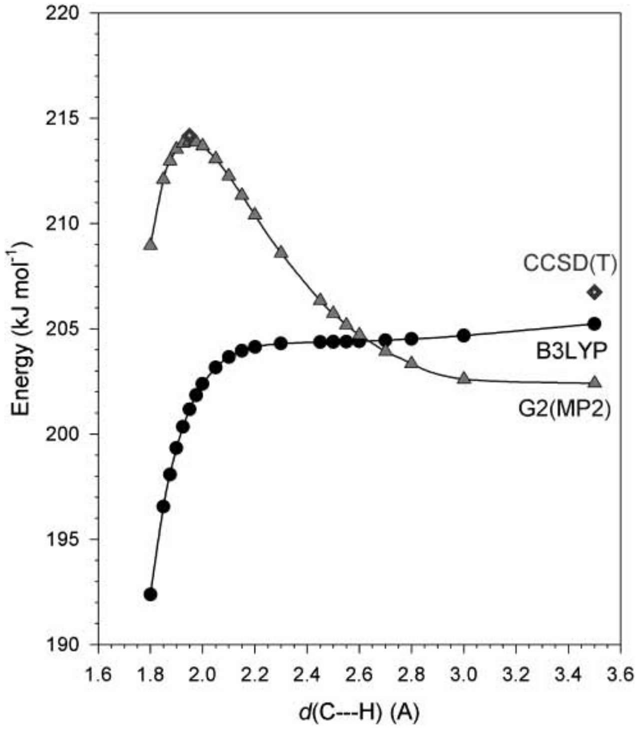

Figure 8. Potential-energy surfaces along the pathway for H−C bond dissociation in **3.** The energies are not corrected for zero-point contributions.

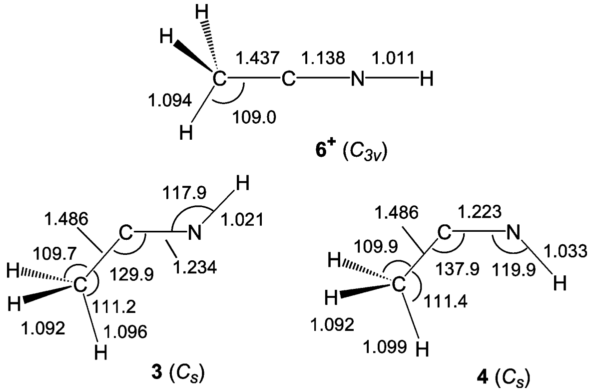

Figure 9. B3LYP/6-311++G(2d,p)-optimized structures. Bond lengths are in angstroms; bond angles are in degrees.

internal energy (E_{ion}), the electronic excitation (E_{exc}), and the excitation due to Franck−Condon effects (E_{FC}). The latter was calculated as 217 and 196 kJ mol^{-1} for the formation of **3** and **4**, respectively. The source of the large E_{FC} is the difference between the equilibrium geometry of **6**$^+$, which has a linear C−C−N−H frame, and those of **3** and **4** that are bent (Figure 9). Substantial differences are also in the C−N bond lengths that contribute to E_{FC}. Table 4 shows that the combined internal energy, $E = E_{\mathrm{ion}} + E_{\mathrm{FC}} \leq 27 + 217 = 244$ kJ mol^{-1}, exceeds the transition-state energies for C−C, N−H, and H−C bond dissociations and can provide the driving force for unimolecular decompositions of **3** and **4**. This explains the very small fraction of survivor **3**/**4** in the NR mass spectra.

The effect on the radical internal energy of vibrational excitation in **6**$^+$ was investigated for the NH bending mode (e_2, 549 cm^{-1}). The potential-energy surface for this bending, calculated by B3LYP/6-311++G(2d,p), showed a harmonic behavior up to $\upsilon = 7$ (Supporting Information, Figure S1). The latter vibrational level corresponded to 45 kJ mol^{-1} excitation in **6**$^+$ and a 125° C−N−H angle. Vertical neutralization of **6**$^+$ from the $\upsilon = 0-7$ vibrational states of the e_2 mode resulted in diminishing Franck−Condon energy in the **3** radical formed (Figure 10, top panel), reaching $E_{\mathrm{FC}} = 110$ kJ mol^{-1} from $\upsilon = 7$. Since e_2 is a low-frequency mode, it can be expected to be significantly populated in $\upsilon > 0$ states in hyperthermal **6**$^+$. Applying Dunbar's formula,[42] we calculate the distribution of vibrational states of the e_2 mode as shown in the bottom panel of Figure 10 for effective vibrational temperatures corresponding to 27 and 58 kJ mol^{-1} internal energy in **6**$^+$. The calculations indicate that vertical neutralization of hyperthermal **6**$^+$ should result in a wide range of excitation energies (110−217 kJ mol^{-1}) in **3** and **4** due to Franck−Condon factors.

RRKM Kinetics. The calculated transition-state energies were further used to calculate unimolecular rate constants for isomerizations and dissociations of **3** and **4**. The kinetic scheme

TABLE 4: Ionization and Recombination Energies[a]

reaction	B3LYP/- 6-311++G(2d,p)	QCISD(T)/- 6-311++G(3df,2p)[b]	G2(MP2)	G2	CCSD(T)/- aug-cc-pVTZ	exp[c]
			$3 \rightarrow 3^+$			
IE_{adiab}	6.41	6.16			6.21	
IE_{vert}	8.18	7.75				
RE_{vert}	3.88				3.94	
			$4 \rightarrow 4^+$			
IE_{adiab}	6.23	5.96			6.01	
IE_{vert}	8.23	7.87				
			$1 \rightarrow 1^{\bullet +}$			
IE_{adiab}	11.87	12.25	12.25	11.15	12.10	12.20

[a] In units of eV. [b] Effective single-point energies, see footnote c in Table 3. [c] From ref 33.

we used takes into account reversible isomerization of **3** and **4** through TS1 and dissociations by loss of H and CH_3 (Scheme 3). Isomerization of **3** to the more stable radical **2** must overcome a substantial barrier (153 kJ mol^{-1})[11] and was therefore considered kinetically unimportant. Laplace transforms[43] and integration of the rate equations that describe Scheme 3 leads to eqs 4−6 for the time-dependent product formations, where c_{N-H}, c_{C-C}, and c_{H-C} are the concentrations of **1**, HNC, and **8**, respectively, c°_{trans} and c°_{cis} are the initial concentrations of **3** and **4**, respectively, t is the dissociation time, and the parameters a, b, k_A, and k_B are defined by eqs 7−10

$$c_{N-H} = \frac{k^{cis}_{N-H}c^{\circ}_{cis}}{a-b}[e^{at} - e^{bt}] + \frac{k^{cis}_{N-H}(c^{\circ}_{cis}k_A + c^{\circ}_{trans}k_{-1})}{a-b}\left[\frac{e^{at}}{a} - \frac{e^{bt}}{b} - \frac{b-a}{ab}\right] \quad (4)$$

$$c_{C-C} = \left[\frac{k^{cis}_{C-C}c^{\circ}_{cis} + k^{trans}_{C-C}c^{\circ}_{trans}}{a-b}\right][e^{at} - e^{bt}] + \frac{k^{cis}_{C-C}(c^{\circ}_{cis}k_A + c^{\circ}_{trans}k_1) + k^{trans}_{C-C}(c^{\circ}_{trans}k_B + c^{\circ}_{cis}k_{-1})}{a-b} \times \left[\frac{e^{at}}{a} - \frac{e^{bt}}{b} - \frac{b-a}{ab}\right] \quad (5)$$

$$c_{H-C} = \frac{k^{trans}_{H-C}c^{\circ}_{trans} + k^{cis}_{H-C}c^{\circ}_{cis}}{a-b}[e^{at} - e^{bt}] + \frac{k^{trans}_{H-C}(c^{\circ}_{trans}k_B + c^{\circ}_{cis}k_{-1}) + k^{cis}_{H-C}(c^{\circ}_{cis}k_A + c^{\circ}_{trans}k_1)}{a-b} \times \left[\frac{e^{at}}{a} - \frac{e^{bt}}{b} - \frac{b-a}{ab}\right] \quad (6)$$

$$a + b = -(k_A + k_B) \quad (7)$$

$$ab = k_A k_B - k_1 k_{-1} \quad (8)$$

$$k_A = k_1 + k^{trans}_{C-C} + k^{trans}_{H-C} \quad (9)$$

$$k_B = k_{-1} + k^{cis}_{N-H} + k^{cis}_{C-C} + k^{cis}_{H-C} \quad (10)$$

The branching ratios $c/\Sigma c$ depend on the reactant internal energy and also on the fraction of **3** and **4** initially produced by neutralization of $\mathbf{6}^+$. The branching ratios that were calculated for $t = 3.3$ μs and $c_{cis}{}^{\circ} = c_{trans}{}^{\circ} = 0.5$ are plotted in Figure 11. The plot shows a rapid disappearance of **3** and **4** at internal energies greater than E_{TS2}. The **1** forming loss of H from **4** dominates at excitations $E \leq 200$ kJ mol^{-1} where there is a crossing point with the C—C bond dissociations in **3** and **4** that prevail at higher internal energies. The position of the crossing point depends on the initial fractions of **3** and **4**. For example, for $c_{cis}{}^{\circ} = 1$ and $c_{trans}{}^{\circ} = 0$, the crossing point appears at $E = 212$ kJ mol^{-1}. The reason for the curve crossing is 2-fold. First, the rate constants for the C—C bond cleavages in **3** and **4** show slightly greater slopes than that of the N—H bond cleavage in **4**. This is caused in part by the significant stiffening of the C═N stretching mode in **TS2** (2226 cm^{-1}) compared to **4** (1816 cm^{-1}) that decreases the number of quantum states in **TS2**. The other reason is that at higher energies the rate constants for C—C bond dissociation in both **3** and **4** become significant and contribute to the convergent formation of H—N═C and CH_3. Also noteworthy is that the fraction of **8** produced by H—C bond dissociation in **3** and **4** remains negligibly small (<0.1%) even at excitations exceeding 300 kJ mol^{-1} (Figure 11). The branching ratios for dissociations of the deuterium-labeled radicals **3a**, **3b**, **3d**, **4a**, **4b**, and **4d** are given as Figures S3−S5 in Supporting Information.

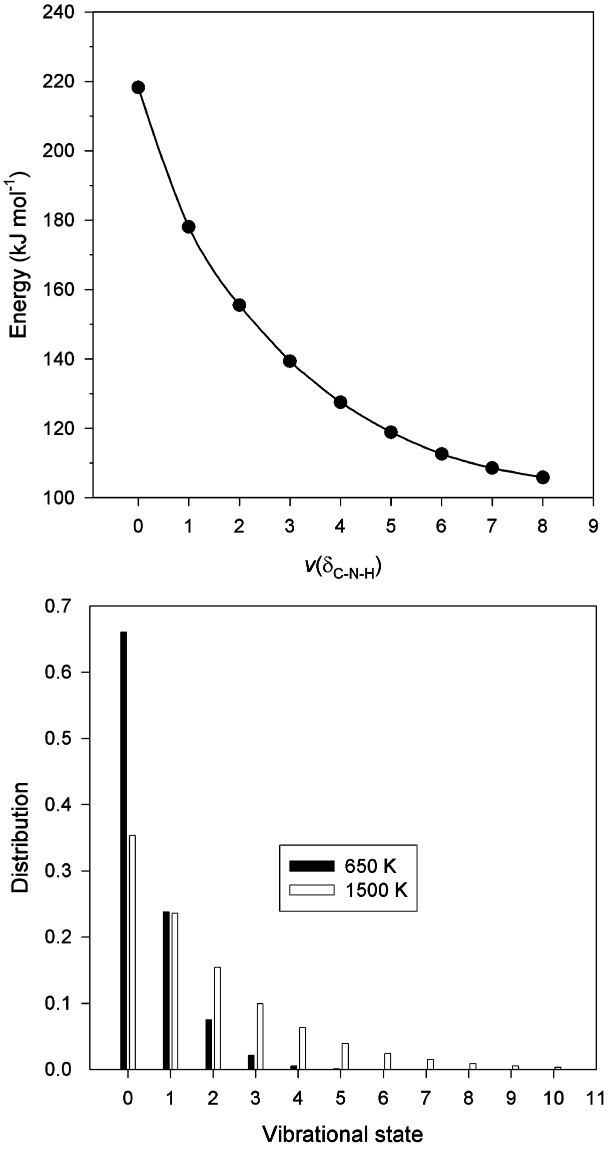

Figure 10. Top panel: Franck−Condon energies in **3** produced by vertical neutralization of $v = 0-8$ vibrational states of the e_2 bending mode (549 cm^{-1}) in $\mathbf{6}^+$. Bottom panel: Distributions of the $v = 0-10$ states in hyperthermal $\mathbf{6}^+$.

To make a quantitative comparison between the RRKM calculated and NR mass spectrometric branching ratios, one has to convolute the former with an internal energy distribution function, $P(E)$. In the past, we used the normalized $P(E)$ function given in eq 11 that was fitted with two parameters, E_0 for onset

$$P(E) = \frac{4(E - E_0)}{W^2} e^{-2(E - E_0)/W} \quad (11)$$

and W for width, such that the most probable energy is at $E_{max} = E_0 + 0.5W$ and the distribution mean is at $\langle E \rangle = E_0 + W$. Convoluting function 11 with eq 4 and 5 gives a fit with the experimental branching ratio for $E_0 = 102$ kJ mol^{-1} and $W = 65$ kJ mol^{-1} for dissociations starting from a 1:1 mixture of **3** and **4**. For dissociations starting from **4**, the best-fit parameters are $E_0 = 102$ kJ mol^{-1} and $W = 75$ kJ mol^{-1}. The onset was chosen at the energy of the lowest transition state (E_{TS2}, 102.6

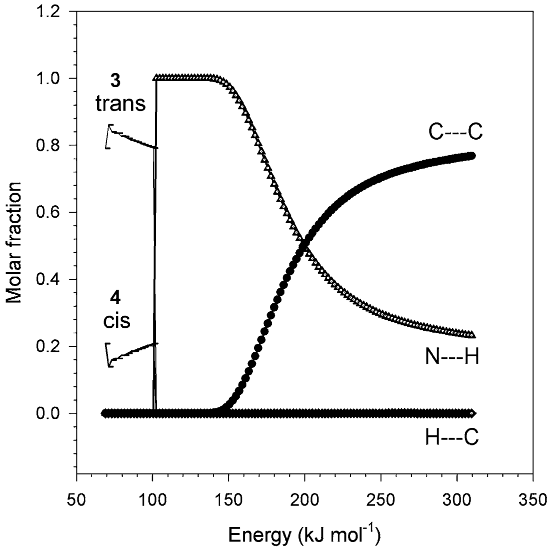

Figure 11. RRKM branching ratios for molar fractions of **3**, **4**, (**1** + H), (**5** + H), and (CH_3 + H−N═C) starting from a 1:1 molar mixture of **3** and **4**.

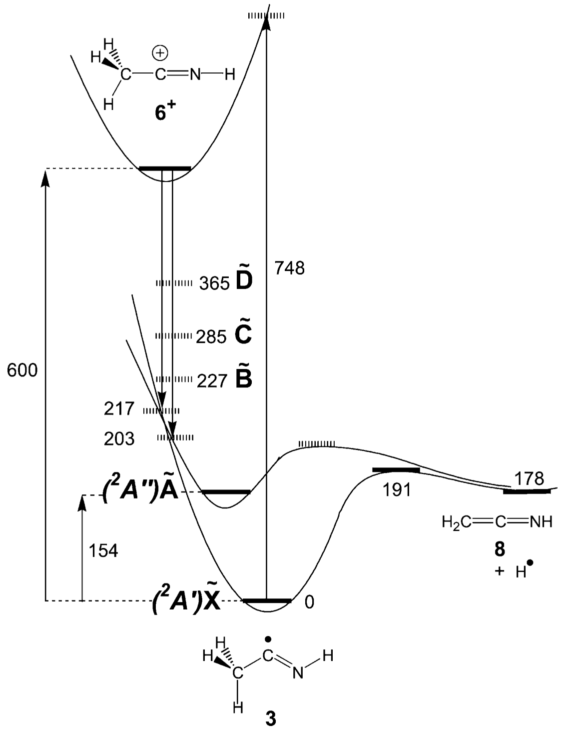

Figure 12. Excited electronic states in **3**. The ionization, recombination, and excitation energies (kJ mol^{-1}) are from TD-B3LYP/6-311++(2d,p) calculations and do not include zero-point corrections. The relative energy of the (^{2}A″) ***A*** state (154 kJ mol^{-1}) is from MP2/6-311++G-(2d,p) optimization.

kJ mol^{-1} relative to **3**) to account for the very small fraction of survivor **3**/**4**.

The kinetic fits show that the branching ratios are not very sensitive to the initial composition of the **3**/**4** mixture. The most probable internal energy, $E_{\max} = E_0 + 0.5W = 177-187$ kJ mol^{-1}, falls within the interval predicted for **3**/**4** on the basis of Franck−Condon energies for neutralization of hyperthermal **6**$^+$. Given the uncertainties in the experimental branching ratios and our neglect of tunnel effects for the loss of H, the agreement between the RRKM data and experiment can be considered satisfactory for competing H and methyl loses. However, the RRKM data do not explain the ~10% fraction of H loss from the methyl group in **3**/**4**.

Excited Electronic States. To account for the loss of H from the methyl group, one has to consider mechanisms other than those included in the RRKM calculations. One possibility is dynamic effects, where the loss of the methyl H may proceed nonergodically from vibrationally excited **3**/**4** of very high internal energy. Such effects have been discovered for a few small neutral[44] and ionic systems[45] and cannot be excluded for **3** and **4**, because the radicals acquire substantial internal energies upon vertical neutralization. However, detailed dynamic calculations for this minor dissociation channel are beyond the scope of the present study. Another possibility that has precedents is dissociation of **3** and **4** from excited electronic states produced by vertical electron transfer. We have addressed this question by perturbational Møller−Plesset and time-dependent B3LYP calculations for **3**, and the results are summarized in Figure 12.

Vertical neutralization of **6**$^+$ can form **3** in a variety of electronic states (Figure 12). The ground (***X***) and first excited state (***A***) are vibrationally excited because of Franck−Condon effects. The ***A*** state of ^{2}A″ symmetry was optimized by MP2/6-311++G(2d,p) and found to be 154 kJ mol^{-1} above the ***X*** state. When formed by vertical electron transfer (at 203 kJ mol^{-1}, Figure 12), the ***A*** state will have ~50 kJ mol^{-1} vibrational energy due to Franck−Condon effects. Note that this is much less than the E_{FC} in the ***X*** state (217 kJ mol^{-1}) and a further decrease of E_{FC} can be expected for vertical formation of the ***B***, ***C***, ***D***, and higher excited states because their equilibrium geometries are likely to resemble that of the ion (Figure 12). Some of these states may be metastable and thus account for the small fraction of survivor **3**/**4** that is observed experimentally. Moreover, vertically formed ***A*** and higher states all have energies that are above the dissociation threshold and TS energy for the loss of H forming **8** (191 kJ mol^{-1}). Thus, the formation of **8** is energetically possible from excited electronic states of **3**. More rigorous mapping of the excited-state potential-energy surface, e.g., by complete active-space calculations, would be necessary to pinpoint the local minima and transition states for loss of H from the methyl group in **3** and **4**. Such calculations are beyond the scope of the present work.

Conclusions

Although 1-azapropen-2-yl radicals are both kinetically and thermodynamically forbidden in thermal radical reactions of acetonitrile, they can be generated transiently by femtosecond electron transfer reduction of stable protonated acetonitrile and are found to dissociate extensively. The branching ratios for the loss of the imine hydrogen and the methyl group are reasonably well reproduced by RRKM calculations on the CCSD(T)/aug-cc-pVTZ potential-energy surface. The occurrence of H-atom loss from the methyl group in competition with the loss of the imine hydrogen is not reproduced by RRKM calculations and probably occurs from an excited electronic state that is produced by electron transfer.

Acknowledgment. Support of this research by the National Science Foundation (Grants CHE-0090930 for experiments and CHE-9808181 and CHE-0342956 for computations) is gratefully acknowledged. The Chemistry Department Computational Facility also received support from the University of Washington. E.A.S. thanks the Alma and Lloyd West Graduate Student Fellowship for support in the course of this work.

Supporting Information Available: Tables S1−S19 of B3LYP/6-311++G(2d,p) with optimized geometries in standard orientation Cartesian coordinate format and Figures S1−S5 with RRKM branching ratios (PDF). This material is available free of charge via the Internet at http://pubs.acs.org.

References and Notes

(1) Jamieson, J. W. S.; Brown, G. R.; Tanner, J. S. *Can. J. Chem.* **1970**, *48*, 3619−3622.

(2) (a) Chandra, H.; Symons, M. C. R. *J. Chem. Soc., Faraday Trans. 1* **1988**, *84*, 3401−3412. (b) Egland, R. J.; Symons, M. C. R. *J. Chem. Soc. A* **1970**, 1326−1329. (c) Mishra, S. P.; Symons, M. C. R. *J. Chem. Soc., Perkin Trans. 2* **1973**, 394−396.

(3) Svejda, P.; Volman, D. H. *J. Phys. Chem.* **1970**, *74*, 1872−1875.

(4) Bigot, B.; Delbecq, F.; Milet, A.; Peuch, V.-H. *J. Catal.* **1996**, *159*, 383−393.

(5) Ditlevsen, P. D.; Gardin, D. E.; Van Hove, M. A.; Somorjai, G. A. *Langmuir* **1993**, *9*, 1500−1503.

(6) Hamm, S.; Warneck, P. *J. Geophys. Res.* **1990**, *95*, 20593−20606.

(7) Tyndall, G. S.; Orlando, J. J.; Wallington, T. J.; Sehested, J.; Nielsen, O. J. *J. Phys. Chem.* **1996**, *100*, 660−668.

(8) Petrie, S. *Icarus* **2001**, *151*, 196−203.

(9) Wang, B.; Hou, H.; Gu, Y. *J. Phys. Chem. A* **2001**, *105*, 156−164.

(10) Balaj, O, P.; Balteanu, I.; Fox-Beyer, B. S.; Beyer, M. K.; Bondybey, V. E. *Angew. Chem., Int. Ed. Engl.* **2003**, *42*, 5516−5518.

(11) Petrie, S. *J. Phys. Chem. A* **2002**, *106*, 11181−11189.

(12) Iraqi, M.; Lifshitz, C. *Int. J. Mass Spectrom. Ion Processes* **1986**, *71*, 245−255.

(13) Anicich, V. G.; Sen, A. D.; Huntress, W. T.; McEwan, M. J. *J. Chem. Phys.* **1995**, *102*, 3256−3261.

(14) (a) Curtis, P. M.; Williams, B. W.; Porter, R. F. *Chem. Phys. Lett.* **1979**, *65*, 296−299. (b) Burgers, P. C.; Holmes, J. L.; Mommers, A. A.; Terlouw, J. K. *Chem. Phys. Lett.* **1983**, *102*, 1−3. (c) Danis, P. O.; Wesdemiotis, C.; McLafferty, F. W. *J. Am. Chem. Soc.* **1983**, *105*, 7454−7456.

(15) For the most recent reviews of the technique, see: (a) Tureček, F. *Top. Curr. Chem.* **2003**, *225*, 77−129. (b) Zagorevskii, D. V.; Holmes, J. L. *Mass Spectrom. Rev.* **1999**, *18*, 87−118. (c) Schalley, C. A.; Hornung, G.; Schroder, D.; Schwarz, H. *Chem. Soc. Rev.* **1998**, *27*, 91−104.

(16) Gilbert, R. G.; Smith, S. C. *Theory of Unimolecular and Recombination Reactions*; Blackwell Scientific Publications: Oxford, 1990; pp 52−132.

(17) Tureček, F.; Gu, M.; Shaffer, S. A. *J. Am. Soc. Mass Spectrom.* **1992**, *3*, 493−501.

(18) Tureček, F. *Org. Mass Spectrom.* **1992**, *27*, 1087−1097.

(19) (a) Kuhns, D. W.; Shaffer, S. A.; Tran, T. B.; Tureček, F. *J. Phys. Chem.* **1994**, *98*, 4845−4853. (b) Kuhns, D. W.; Tureček, F. *Org. Mass Spectrom.* **1994**, *29*, 463−469.

(20) Frisch, M. J.; Trucks, G. W.; Schlegel, H. B.; Scuseria, G. E.; Robb, M. A.; Cheeseman, J. R.; Zakrzewski, V. G.; Montgomery, J. A., Jr.; Stratmann, R. E.; Burant, J. C.; Dapprich, S.; Millam, J. M.; Daniels, A. D.; Kudin, K. N.; Strain, M. C.; Farkas, O.; Tomasi, J.; Barone, V.; Cossi, M.; Cammi, R.; Mennucci, B.; Pomelli, C.; Adamo, C.; Clifford, S.; Ochterski, J.; Petersson, G. A.; Ayala, P. Y.; Cui, Q.; Morokuma, K.; Malick, D. K.; Rabuck, A. D.; Raghavachari, K.; Foresman, J. B.; Cioslowski, J.; Ortiz, J. V.; Stefanov, B. B.; Liu, G.; Liashenko, A.; Piskorz, P.; Komaromi, I.; Gomperts, R.; Martin, R. L.; Fox, D. J.; Keith, T.; Al-Laham, M. A.; Peng, C. Y.; Nanayakkara, A.; Gonzalez, C.; Challacombe, M.; Gill, P. M. W.; Johnson, B. G.; Chen, W.; Wong, M. W.; Andres, J. L.; Head-Gordon, M.; Replogle, E. S.; Pople, J. A. *Gaussian 98*, revision A.6; Gaussian, Inc.: Pittsburgh, PA, 1998.

(21) (a) Becke, A. D. *J. Chem. Phys.* **1993**, *98*, 1372−1377. (b) Becke, A. D. *J. Chem. Phys.* **1993**, *98*, 5648−5652. (c) Stephens, P. J.; Devlin, F. J.; Chabalowski, C. F.; Frisch, M. J. *J. Phys. Chem.* **1994**, *98*, 11623−11627.

(22) (a) Schlegel, H. B. *J. Chem. Phys.* **1986**, *84*, 4530−4534. (b) Mayer, I. *Adv. Quantum Chem.* **1980**, *12*, 189−262.

(23) Curtiss, L. A.; Raghavachari, K.; Pople, J. A. *J. Chem. Phys.* **1993**, *98*, 1293−1298.

(24) Curtiss, L. A.; Raghavachari, K.; Trucks, G. W.; Pople, J. A. *J. Chem. Phys.* **1991**, *94*, 7221−7230.

(25) Čížek, J.; Paldus, J.; Šroubková, L. *Int. J. Quantum Chem.* **1969**, *3*, 149−167.

(26) Purvis, G. D.; Bartlett, R. J. *J. Chem. Phys.* **1982**, *76*, 1910−1918.

(27) Dunning, T. H., Jr. *J. Chem. Phys.* **1989**, *90*, 1007−1023.

(28) Stratmann, R. E.; Scuseria, G. E.; Frisch, M. J. *J. Chem. Phys.* **1998**, *109*, 8218−8224.

(29) Foresman, J. B.; Head-Gordon, M.; Pople, J. A.; Frisch, M. J. *J. Phys. Chem.* **1992**, *96*, 135−149.

(30) Zhu, L.; Hase, W. L. *Quantum Chemistry Program Exchange*; Indiana University: Bloomington, 1994; Program No. QCPE 644.

(31) Frank, A. J.; Sadílek, M.; Ferrier, J. G.; Tureček, F. *J. Am. Chem. Soc.* **1997**, *119*, 12343−12353.

(32) The reaction enthalpy in eq 3 is based on the standard enthalpies of formation (kJ mol^{-1}) for **1** (74),[33] CH$_2$CN (253),[34] and the adiabatic ionization energy (1177) and proton affinity (779) of **1**.[32]

(33) NIST Standard Reference Database No. 69. February 2000 release. http://webbook.nist.gov.

(34) Lafleur, R. D.; Szatary, B.; Baer, T. *J. Phys. Chem. A* **2000**, *104*, 1450−1455.

(35) Harrison, A. G. *Chemical Ionization Mass Spectrometry*, 2nd ed.; CRC Publishers: Boca Raton, 1992; pp 15−17.

(36) Mayer, P. M. *J. Phys. Chem. A* **1999**, *103*, 3687−3692.

(37) (a) Würthwein, E.-U. *J. Org. Chem.* **1984**, *49*, 2971−2978. (b) Nguyen, M. T.; Ha, T.-K. *J. Chem. Soc., Perkin Trans. 2* **1984**, 1401−1405. (c) Bonnet-Delpon, D.; Charpentier-Morize, M.; Loupy, A. *Chem. Phys. Lett.* **1985**, *116*, 478−481. (d) Malone, S.; Hegarty, A. F.; Nguyen, M. T. *J. Chem. Soc., Perkin Trans. 2* **1988**, 477−483. (e) Botschwina, P. *J. Mol. Spectrosc.* **2000**, *203*, 203−204.

(38) A reviewer suggested that energetic CH$_3$CN$^{\bullet+}$ could isomerize to the comparably stable CH$_3$NC$^{\bullet+}$ that could abstract a hydrogen atom from CH$_3$CN forming CH$_3$N═C−H$^+$ (**9**$^+$) that would contaminate the ion beam of **6**$^+$. However, according to our calculations, ion **9**$^+$ can undergo an exothermic reaction with CH$_3$CN yielding CH$_3$C═N−CH$_3$$^+$ (**10**$^+$, Table 1) that should deplete the population of the undesirable ion isomer. By contrast, a methyl transfer to CH$_3$CN from **6**$^+$ is endothermic (Table 1) making this isomer unreactive under the conditions of ion−molecule reactions in the ion source.

(39) Leeck, D. T.; Kenttamaa, H. I. *Org. Mass Spectrom.* **1994**, *29*, 106−107.

(40) Nguyen, V. Q.; Tureček, F. *J. Mass Spectrom.* **1996**, *31*, 843−854.

(41) Fitch, W. L.; Sauter, A. D. *Anal. Chem.* **1983**, *55*, 832−835.

(42) Dunbar, R. C. *J. Chem. Phys.* **1989**, *90*, 7369−7375.

(43) Benson, S. W. *The Foundations of Chemical Kinetics*; McGraw-Hill: New York, 1960; p 29.

(44) (a) Rynbrandt, J. D.; Rabinovitch, B. S. *J. Phys. Chem.* **1970**, *74*, 4175−4176. (b) Oref, I.; Rabinovitch, B. S. *Acc. Chem. Res.* **1979**, *12*, 166−175.

(45) (a) McLafferty, F. W.; McAdoo, D. J.; Smith, J. S.; Kornfeld, R. *J. Am. Chem. Soc.* **1971**, *93*, 3720−3730. (b) Depke, G.; Lifshitz, C.; Schwarz, H.; Tzidony, E. *Angew. Chem., Int. Ed. Engl.* **1981**, *20*, 792−793. (c) Tureček, F.; McLafferty, F. W. *J. Am. Chem. Soc.* **1984**, *106*, 2525−2528. (d) Tureček, F.; Hanuš, V. *Org. Mass Spectrom.* **1984**, *19*, 631−638. (e) Nummela, J. A.; Carpenter, B. K. *J. Am. Chem. Soc.* **2002**, *124*, 8512−8513.